Contents lists available at ScienceDirect

Atmospheric Environment: X
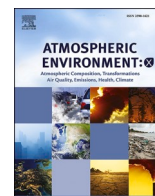
Chemical and physical characterization of oil shale combustion emissions in Estonia

Minna Aurela [a,b,*], Fanni Mylläri [b], Alar Konist [c], Sanna Saarikoski [a], Miska Olin [b], Pauli Simonen [b], Matthew Bloss [a], Dmitri Nešumajev [c], Laura Salo [b], Marek Maasikmets [d], Mikko Sipilä [e], Miikka Dal Maso [b], Jorma Keskinen [b], Hilkka Timonen [a], Topi Rönkkö [b]

[a] Atmospheric Composition Research, Finnish Meteorological Institute, P.O. Box 503, FI-00101, Helsinki, Finland
[b] Aerosol Physics Laboratory, Faculty of Engineering and Natural Sciences, Tampere University, P.O. Box 692, FI-33014, Tampere University, Finland
[c] Department of Energy Technology, Tallinn University of Technology, 19086, Tallinn, Estonia
[d] Air Quality Management Department, Estonian Environmental Research Center, 10617, Tallinn, Estonia
[e] Institute for Atmospheric and Earth System Research /Physics, Faculty of Science, University of Helsinki, Helsinki, FI-00014, Finland

ARTICLE INFO

ABSTRACT

In this study, oil shale combustion emission measurements were conducted in a 60 kW$_{th}$ Circulating Fluidized Bed combustion test facility located in a laboratory-type environment. A comprehensive set of instruments including a nitrate-ion-based Chemical Ionization Atmospheric Pressure interface Time-of-Flight Mass Spectrometer, a Soot-Particle Aerosol Mass Spectrometer, and a Potential Aerosol Mass (PAM) chamber was utilized to investigate the chemical composition and concentrations of primary and secondary emissions in oil shale combustion. In addition, the size distribution of particles (2.5–414 nm) as well as concentration and composition of gaseous precursors were characterized. Altogether 12 different experiments were conducted. Primary emissions were studied in seven experiments and aged emissions using PAM chamber in five experiments. Combustion temperatures and solid fuel circulation rates varied between different experiments, and it was found that the burning conditions had a large impact on gaseous and particulate emissions. The majority of the combustion particles were below 10 nm in size during good burning whereas in poor burning conditions the emitted particles were larger and size distributions with 2–3 particle modes were detected. The main submicron particle chemical component was particulate organic matter (POM), followed by sulfate, chloride, nitrate, and ammonium. The secondary particulate matter formed in the PAM chamber was mostly POM and the concentration of POM was many orders of magnitude higher in aged aerosol compared to primary emissions. A significant amount of aromatic volatile organic compounds (VOCs) was measured as well. VOCs have the potential to go through gas-to-particle conversion during the oxidation process, explaining the observed high concentrations of aged POM. During good combustion, when VOC emissions were lower, over 80% of SO_2 was oxidized either to gaseous H_2SO_4 (37%) or particulate sulfate (46%) in the PAM chamber, which mimic the atmospheric processes taken place in the ambient air after few days of emission.

1. Introduction

Environmental policies of the European Union (EU) aim to decrease carbon dioxide emissions originating from fossil fuel combustion, restrain energy demand, and optimize resource consumption. The EU Emissions Trading System (EU ETS) sets an overall limit on all fossil CO_2 emissions from power stations, energy-intensive industries, and civil aviation. Until 2019, Estonia has received decreasing number of free carbon allowances for power producers for modernizing their electricity sectors. Over 70% of the energy is produced in Estonia by oil shale combustion and oil shale will remain an important fuel also during the period 2021–2030. In addition to produce greenhouse gases and harmful gaseous emissions, combustion of oil shale is releasing particles into the atmosphere. Combustion based particles are known to be harmful to human health and they have direct and indirect climate effects (e.g., Lelieved et al., 2015; Andrea et al., 2005).

Oil shale is sedimentary rock containing up to 50% of organic matter and it has a high mineral content; around 40–50% of the original mass remains even after combustion. Once extracted from the ground, the rock can either be used directly as a power plant resource or be processed to produce shale oil and other chemicals and materials (Strizhakov and Usova, 2008). Considerable quantities of oil shale are mined in Estonia, Russia, China, Brazil, Australia, and Germany. Estonian oil shale (kerogen) is a very difficult-to-burn fuel due to its unique properties. It has high alkali and chlorine content. The content of sulfur is up to 2%. (Konist et al., 2013).

In Estonia, the Pulverized Combustion (PC) and Circulating Fluidized Bed Combustion (CFBC) technologies are used for power production. Mainly due to the ageing of PC boilers but also because of environmental and economic problems, the old power units are being decommissioned. This is supported by government policy so that by the end of 2023 all such PC units must be permanently closed down since the environmental impact of CFBC is significantly less than that of PC (Konist et al., 2019).

Currently electrostatic precipitators (ESP) are used in the older industrial CFB boilers, where the particulate matter content can be up to 20 mg Nm^{-3} (6% O_2, dry gases, EU, 2010). Due to stringent environmental legislation, both ESP and fabric filters were installed for the new power plants to achieve a dust content below 10 mg Nm^{-3} (6% O_2, dry gases, Directive, 2010/75/EU). The concentration of SO_2 in the flue gas is almost negligible because nearly all of the sulfur is bound by free CaO in the ash. No other flue gas cleaning systems for $DeNO_x$ and $DeSO_x$ are needed because of the fuel properties and combustion technology utilized (Pihu et al., 2017). The improved efficiency and decreased carbonate decomposition in CFBC have decreased the CO_2 emissions per produced power unit by nearly 24% (Pihu et al., 2017).

In this study, oil shale combustion measurements were conducted in the 60 kW$_{th}$ CFB combustion test facility in Tallinn University of Technology, Estonia. A comprehensive set of sophisticated instruments, such as a nitrate-ion-based Chemical Ionization Atmospheric Pressure interface Time-of-Flight Mass Spectrometer (CI-APi-ToF), a Soot-Particle Aerosol Mass Spectrometer (SP-AMS), and a Potential Aerosol Mass (PAM) chamber, was utilized to investigate the primary and secondary emissions of oil shale combustion. The main goal of the study was to characterize physico-chemical properties of submicron particles, sulfuric acid formation and aging behavior of aerosols emitted from oil shale combustion. Some studies concerning characterization of solid oil shale and its ash, composition of gaseous components (e.g., methane, non-methane hydrocarbons, SO_2) and particulate matter mass concentration ($PM_{2.5}$, PM_{10}) of flue gas from oil shale combustion have been presented earlier (e.g. Maaten et al., 2020; Parve et al., 2011; Martins et al., 2010*t al.*), but to our knowledge, there are no peer-reviewed articles with on-line chemical and physical characterization of particles during oil shale combustion.

2. Experimental

2.1. Circulating Fluidized Bed test facility

The CFB test facility located in Tallinn University of Technology, Estonia enabled combustion of typically low calorific fuels (oil shale, biomass, lignite, and coal) and their mixtures. The facility closely resembled the power stations used for oil shale combustion. The only notable difference between power stations and the test facility was the flue gas cleaning system setup. The test facility only used fabric filters whereas power stations use a combination of fabric filters and electrostatic filters.

The main components of the CFB are shown in Fig. S1 and explained shortly in the Supplementary Material. During the experiments, burning conditions with different temperatures (500–1000 °C) and solid circulation rates were varied. Typically, the increase of solid circulating rate decreased the temperature in the furnace. The large temperature variation may indicate issues in burning conditions like additional

adjustments in solid circulation rate or unstable fuel addition. Combustion efficiency, which describes how completely the fuel has burned, was calculated from CO and CO_2 concentrations (ppm) by dividing CO_2 by the sum of CO and CO_2 (see 2.2.4.). The average combustion efficiency varied between 0.82 and 0.97 during the experiments (Table 1).

12 sub-experiments (duration: 10–72 min) were separated from the whole burning experiment (Table 1). They were named chronically and based on the status of the burning (Good, Fair, and Poor). Either high, low, or large variation in furnace temperature were named Poor; stable temperature around 700 °C were named Good, and the rest of experiments were named Fair.

2.2. Instrumentation

The instrumentation used in the measurements is described in Fig. S2 and their operating principles and parameters are explained shortly below. A double-ejector system (Dekati Ltd., Finland) was used for diluting the flue gas. The first diluter used dilution air heated to 70 °C and the second one was operating at the room temperature. The dilution ratio (DR) was calculated based on the observed ratios of gas concentrations, mainly from the CO_2 concentration at raw emissions and after the ejectors. The average DR over the two ejectors was approximately 80.

2.2.1. Potential Aerosol Mass chamber

An oxidation flow reactor, PAM chamber, was used to simulate the secondary aerosol formation potential of the flue gas in the atmosphere (Kang et al., 2007). Potential aerosol mass is defined as the maximum aerosol mass that is produced when the precursor gases (and primary particles) are oxidized in the PAM chamber. The UV lamps inside the chamber emitted both 185 nm and 254 nm UV radiation (Peng and Jimenez, 2020) producing O_3, and OH- and HO_2-radicals. OH-radicals are typically the main oxidants in the atmosphere (Lambe et al., 2011). The OH exposure during the measurements was modeled in a similar manner as in Timonen et al. (2017) and explained in the Supplementary Material.

The average sample residence time in the chamber with a flow rate of 6.6 L min^{-1} was 121 s. The chamber flow was divided to inner (5.1 L min^{-1}) and ring flow (1.5 L min^{-1}). The latter was used to reduce the sample interactions with the walls, and it was diverted to exit through an internal perforated ring that dumps air near the reactor walls. After exiting the chamber, the inner flow was further diluted using an ejector after the chamber (DR: 12–13) to get a large enough sample flow rate for the instruments. This additional dilution step after the PAM may shift the partitioning of the semivolatile species towards the gas phase

Table 1
Description of the combustion (Good, Fair, Poor) and combustion parameters (T, Combustion efficiency, CO_2 raw) during different experiments. CO_2 raw was measured from the raw gas before the dilution. T1 represents the temperature in the bottom of the furnace (see Fig. S1). The number after the name shows the chronological order of the experiment.

Experiment	T1 avg ± stdev (°C)	T range (°C)	ΔT (°C)	Combustion efficiency[a]	CO_2 raw (vol %)
Fair 1	639 ± 14	601–658	57	0.85	1.72
Fair 2	685 ± 120	454–896	442	0.87	2.00
Fair 3	631 ± 31	563–691	128	0.86	2.03
Fair 4	742 ± 23	669–806	137	0.96	2.10
Poor 5	824 ± 11	800–849	49	0.97	3.26
Good 6	712 ± 19	678–740	62	0.92	1.71
Good 7	708 ± 63	547–765	218	0.91	1.68
Fair 8	546 ± 45	471–609	138	0.84	1.37
Poor 9	517 ± 97	353–774	421	0.82	1.46
Poor 10	515 ± 39	434–634	200	0.82	3.08
Poor 11	503 ± 68	360–719	359	0.82	2.58
Poor 12	755 ± 103	549–921	372	0.97	5.30

[a] Combustion efficiency: CO_2 [ppm]/(CO_2+CO) [ppm].

(Lipsky and Robinson, 2006). Primary emissions (without PAM) or aged particles (with PAM) were measured alternately in approximately 30 min time intervals. During the bypass flow, the ring flow and ejector suction through the chamber was maintained to keep constant flow through the chamber. Primary particle losses for a PAM chamber with similar dimensions as used here have been shown to be generally small especially in the particle sizes that contain most of the aerosol mass (15% at 100 nm and below 10% above 150 nm; Karjalainen et al., 2016).

2.2.2. Soot-Particle Aerosol Mass Spectrometer

Overall aerosol chemical composition and particle size resolved chemical composition were measured with a SP-AMS (Aerodyne Research Inc, Onasch et al., 2012) with a time-resolution of 1-min. The SP-AMS measures at its measurement size range ($\sim$50–800 nm) non-refractory species i.e., sulfate, nitrate, ammonium, chloride, and POM but also refractory black carbon (rBC) and some metals due to an additional laser vaporizer. The rBC is the sum of carbon ions (e.g., C_1, C_2 and C_3). However, rBC concentrations are not presented in this study as there were high contributions of organic carbon ions to C_2 and C_3 when aged particles were measured. The contribution of rBC for primary particulate matter during a good burning condition was on average 7%.

Quantification of the AMS results requires application of a collection efficiency (CE) to account for e.g., particle bounce at the tungsten vaporizer of the AMS (Canagaratna et al., 2007; Middlebrook et al., 2012). Typical values range from 0.5 to 1. For ambient aerosols, CE can be estimated from aerosol chemical composition (Middlebrook et al., 2012); however, that parameterization does not always apply to laboratory studies, when inorganic signals are very low relative to organic mass or if the laser is used as a vaporizer, such as in this study (Docherty et al., 2013; Willis et al., 2014). CE of 1 was used in this study, implying that the results can be taken as the lower limit for the concentrations. Elemental analysis was applied to the AMS organic aerosol (OA) measurements to yield the atomic ratios of oxygen-to-carbon (O/C) and hydrogen-to-carbon (H/C) (Aiken et al., 2008; Canagaratna et al., 2015).

In the AMS, the concentrations are calculated based on the subtractions between total ions (containing gaseous and particulate matter) and gaseous components. One of the main gaseous components is CO_2, which is quite constant in the ambient atmosphere ($\sim$400 ppm) but may vary substantially in emission measurements. The gaseous CO_2 concentrations varied roughly between 150 and 800 ppm at the sampling point when measuring primary particles. For the aged particles, the gaseous CO_2 concentration at the sampling point was roughly 10–40 ppm as the dilution ratio was quite high. Flue gas was diluted with synthetic air, which did not contain any CO_2. In this study, the data was corrected with the measured gaseous CO_2 concentration for the aged particles, but for the primary emissions, the concentration of particulate CO_2^+ was assumed to be close to zero and therefore all CO_2-related ions were excluded from the calculation of organic matter. Typically, aged particles have high contribution of fragment ion of CO_2^+ because of the oxidation processes whereas primary particles do not have that ion fragment (e.g. Crippa et al., 2013).

2.2.3. Chemical Ionization Atmospheric Pressure interface time-of-Flight Mass Spectrometer

A nitrate-ion-based CI-APi-ToF (Aerodyne Research Inc.) was used for measuring sulfuric acid molecules and clusters. The APi-ToF and the used CI-inlet are described in-detail elsewhere (Junninen et al., 2010; Jokinen et al., 2012) and are presented here shortly. Nitrate ions were created by exposing clean nitrogen gas (20 L min^1) containing trace levels of nitric acid vapor to X-ray source. Nitrate ions in the sheath flow were directed into the sample flow (10 L min^{-1}) by means of an electric field. The calculated penetration efficiencies of hydrated H_2SO_4 for the bypassing line and through the PAM chamber line were $(4.4 \pm 1.2)10^{-4}$ and $(9 \pm 5)10^{-4}$, respectively (details on the calculation can be found in the Supplementary Material).

Data were recorded with 1-s time resolution, but signals were

averaged over 1 min. The sulfuric acid concentration was calculated based on the sum of sulfuric acid monomer, dimer, and bisulfate ion – nitric acid cluster divided by the sum of nitrate ion monomer, dimer, and trimer. The most abundant sulfuric acid signal was the monomer (HSO_4^-) followed by bisulfate ion - nitric acid cluster and sulfuric acid dimer (Fig. S3). The resulting quotients were then multiplied with a calibration coefficient of 1.3×10^9 molecules cm^{-3} determined in the laboratory after the experiment based on the procedure presented by Kürten et al. (2012).

2.2.4. Auxiliary measurements

Number size distributions of the particles were measured with two scanning mobility particle sizers (SMPS) consisting of an electrostatic classifier, a differential mobility analyzer (DMA, model DMA3085, TSI Ltd.) and a condensation particle counter (CPC, model CPC3776, TSI Ltd.) in the nano-SMPS and a DMA3081 (TSI Ltd.) and a CPC3775 (TSI Ltd.) in the long-SMPS that together covered particle sizes of 2.5–414 nm. The number size distributions measured by the SMPSs were converted to mass size distributions by using calculated gravimetric density values ranging 0.95–1.46 g cm^{-3}. The gravimetric density was calculated based on the chemical composition measured by the SP-AMS with the assumptions that particle density did not change with particle size and the majority of the emitted submicron particles were analyzed by the SP-AMS (COST Action CA1609). For sulfate, ammonium and nitrate the density value of 1.75 g cm^{-3}, for chloride 1.52 g cm^{-3} and for BC 1.77 g cm^{-3} were used (Poulain et al., 2014). For density calculation, 7% contribution of BC for all the primary particles was used (see 2.2.2). The contribution of BC for aged particles was considered to be negligible. The density of POM was calculated based on the elemental ratio and it varied between 0.92 and 1.42 g cm^{-3} (Table 2, Kuwate et al., 2012). The gravimetric density value may differ from the effective density value that can be estimated, for example by comparing the size distribution of aerodynamic and mobility diameters. For example, effective density values of 2–3 g cm^{-3} and close to unity have been presented in coal combustion and at urban environments, respectively (e.g., Mylläri et al., 2016, 2017; Geller et al., 2006).

Trace gas concentrations were measured with a Fourier transform infrared spectroscopy (FTIR), from the raw gas and just before the PAM chamber, thus they represented primary emissions. For this application the FTIR just before PAM chamber was configured for inorganic

Table 2
The average submicron mass concentrations, H:C, O:C, POM:OC elemental ratios, oxidation states (OSc) and estimated density of organic for different experiments during oil-shale combustion experiments. For aged particles, the modeled OH exposure in days is in the parentheses.

Experiment PRIMARY	Organics (mg m^{-3})	H:C	O:C	OSc[a]	POM: OC	Estimated density of POM [g cm^{-3}][b]
Fair 1	0.003	1.52	0.32	−0.89	1.57	1.17
Fair 3	0.008	1.39	0.35	−0.70	1.59	1.23
Poor 5	0.058	1.65	0.15	−1.36	1.34	1.01
Good 6	0.004	1.32	0.32	−0.67	1.56	1.24
Fair 8	0.003	1.87	0.19	−1.48	1.42	0.99
Poor 10	2.999	1.77	0.06	−1.65	1.23	0.92
Poor 12	0.471	1.74	0.07	−1.61	1.24	0.93
AGED						
Fair 2 (2.2 d)	241	1.85	0.65	−0.55	2.02	1.28
Fair 4 (5.0 d)	162	1.82	0.75	−0.32	2.15	1.34
Good 7 (8.7 d)	75	1.82	0.89	−0.04	2.33	1.42
Poor 9 (1.6 d)	408	1.88	0.51	−0.87	1.83	1.19
Poor 11 (4.2 d)	358	1.90	0.63	−0.64	1.99	1.25

[a] OSc (oxidation state of organics) $\approx$ 2 O/C – H/C (Kroll et al., 2011).
[b] ρ_{org} = [(12 + 1(H:C) + 16(O:C)]/[7.0 + 5.0(H:C) + 4.15(O:C)] (Kuwata et al., 2012).

combustion gas components such as CO, NO, NO$_2$, N$_2$O, SO$_2$, HCl, NH$_3$, H$_2$O and CO$_2$ as well as a number of organic species such as CH$_4$, C$_2$H$_6$, C$_2$H$_4$, HCHO and some aromatic compounds. From the raw gas CO, SO$_2$, H$_2$O, and CO$_2$ were measured. CO$_2$ was used for calculating the DR.

3. Results and discussion

Altogether 12 experiments were extracted from the whole burning experiment. Seven of them (Fair 1, Fair 3, Poor 5, Good 6, Fair 8, Poor 10, and Poor 12) represented primary particulate and gaseous emissions. In five experiments (Fair 2, Fair 4, Good 7, Poor 9, and Poor 11), the samples were oxidized in the PAM chamber to measure aged particulate emission and primary gaseous emissions. In the PAM chamber, precursor gases were oxidized, and new particles may form through nucleation or oxidized gases may condense on the top of the existing particles. Two experiments were selected to represent good burning conditions: Good 6 for primary particles and Good 7 for aged particles. Five experiments were categorized to poor burning (Poor 5, Poor 9, Poor 10, Poor 11, and Poor 12) and others to fair burning (Fair 1, Fair 2, Fair 3, Fair 4, and Fair 8) (Table 1).

3.1. Number and mass size distributions

A large variation in concentrations and size distributions of particulate emissions were observed depending on burning conditions. During the experiments the total number concentrations of primary particles in the flue gas varied between 10^4 and 10^7 particles cm^{-3}. Most of the emitted particles were only a few nm in size, being clearly out of the measurable size range of the SP-AMS. However, the observed number and mass size distributions varied quite a lot between the different

primary particle experiments (Fig. 1). For example, in Good 6, Fair 1, and Fair 8 (Fig. 1, left panel) the majority of the particles were below 10 nm in size and the modal diameter of the number size distribution appeared to be below the measured size range. For other primary particle experiments, two to three particle modes were detected within the measured size range. When looking at the mass size distribution of primary particles during poor combustion (Poor 5, Poor 10, and Poor 12), it displayed a bimodal distribution, with the nucleation and accumulation modes peaking approximately at 6–30 nm and 100 nm, respectively (Fig. 1, middle panel). In the latter mode the particles were large enough to be measured by the SP-AMS and high mass concentrations were detected by the SP-AMS for the poor combustion experiments (Fig. 2, middle panel). The experiment Fair 3 differed from the others as it had only one distinct mode at 20–30 nm. For aged particles (Fig. 1, right panel), the number and mass size distributions with only one broad mode peaking at 60 and 100 nm were observed. Note that the aged particles measured with the PAM do not represent the size distribution in a real ambient atmosphere where also particles and gases emitted from sources other than oil shale combustion take part in the atmospheric processes.

Compared to coal or heavy oil combustion in power plants, the dominating particle number size distribution mode for coal combustion in a pulverized fuel-fired power plant boiler has been shown to be unimodal peaking at 25–31 or 80 nm depending on the used flue gas cleaning conditions (Mylläri et al., 2016, 2017), whereas in industrial heavy oil combustion the number size distribution has been bimodal with the dominating mode peaking at ca. 50 nm and another mode at 120 nm (Happonen et al., 2013). In our oil shale combustion experiments, the number size distribution had modes at smaller sizes. The smallest mode was around 10 nm and the larger mode above 40 nm in
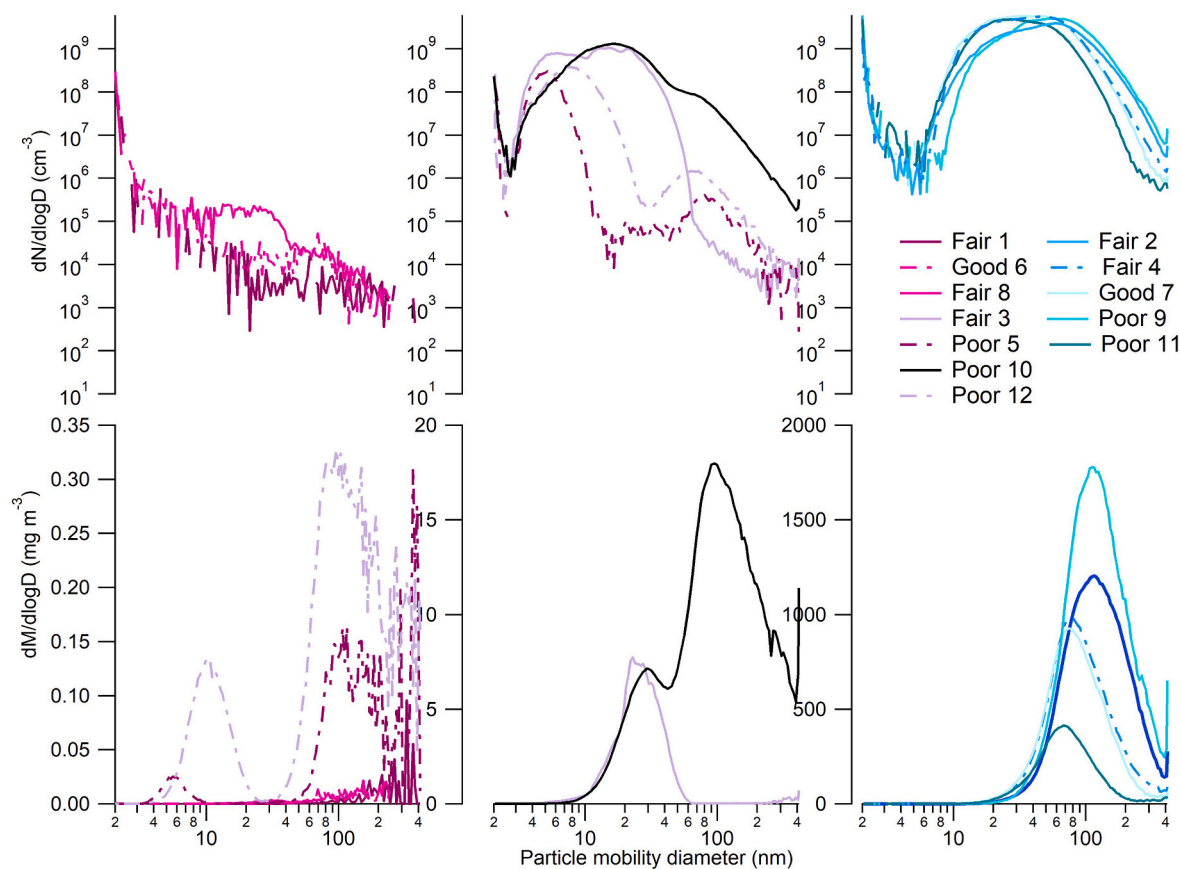

Fig. 1. Number (upper) and calculated mass (lower) size distributions of oil shale combustion emissions measured by the SMPS. Left and middle columns present primary emission experiments (Fair 1, Fair 3, Poor 5, Good 6, Fair 8, Poor 10, and Poor 12) whereas experiments Fair 2, Fair 4, Good 7, Poor 9, and Poor 11 (right columns) were measured after the PAM (aged particle matter). Note the logarithmic scale for x-axes and upper y-axes.
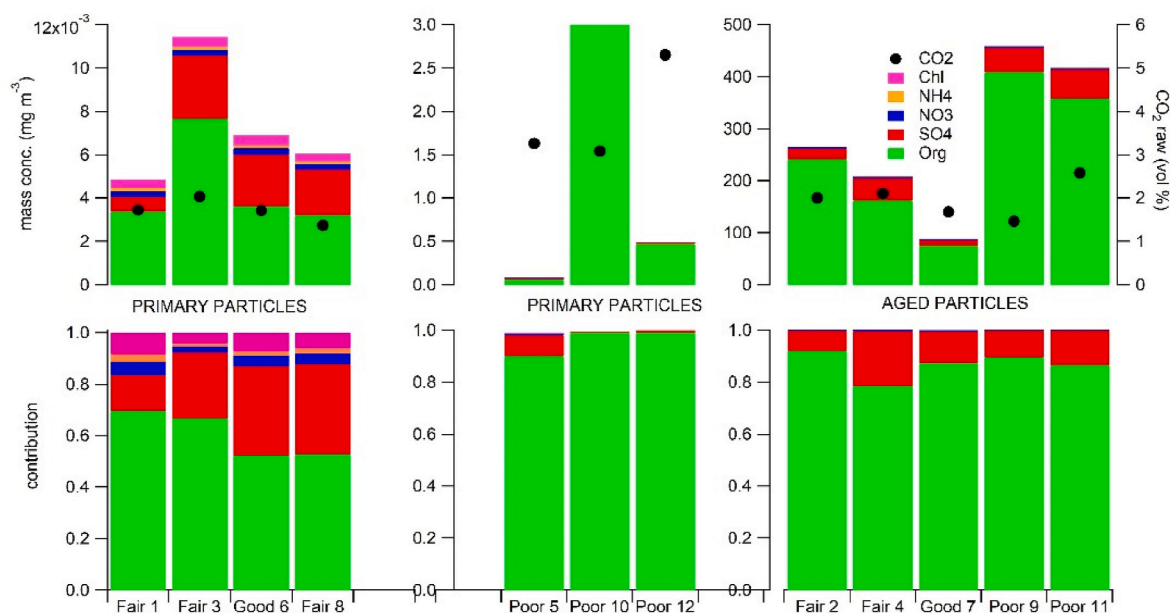
Fig. 2. Concentrations (upper panel) and contributions (lower panel) of main chemical components in submicron particles for primary experiments (left and middle) and aged particles (right) during oil-shale combustion. Note the different scales of the concentration axis for the upper panels.

the experiments Poor 5 and Poor 12. An additional mode around 20 nm had the experiments Poor 10 and Fair 3. However, during the primary particle experiment with good burning conditions (Good 6) or most of the primary particle experiments with fair burning conditions, no clear modes were observed, indicating that the burning conditions affected particulate emissions considerably. When looking at the mass or volume size distributions, coal combustion has produced a unimodal mass size distribution with the volumetric mean mode size of 35 nm (Mylläri et al., 2017) that is close to the size detected in the experiment Fair 3. However, the mass size distribution for other experiments was bimodal in the analyzed size range. In heavy oil combustion, only one mode in volume distribution at 480 nm in aerodynamic diameter has been detected (Happonen et al., 2013) that is close to the size range limit in the SMPS system. In this study, the calculated mass size distribution seemed to have another mode above the analyzed size range of the SMPS systems as there was an increasing trend above 400 nm size in many of the experiments (Fig. 1). The size distribution of POM measured with the SP-AMS had a distinct mode at 400–600 nm (vacuum aerodynamic diameter) in the experiment Poor 10, which had the highest mass concentration among the primary particle experiments (not shown). For other primary particle experiments, the mass concentrations of POM were not high enough to produce representative size distribution. As a summary, oil shale combustion clearly produced a different size distribution profile than coal or heavy oil combustion. However, one should note that there was considerable variation in the measured number size distribution for this test facility.

3.2. Chemical composition of particles

The mass concentrations and contributions of main components in the analyzed submicron particulate matter for different experiments are presented in Fig. 2. Particle mass concentrations of PM10 were also measured during this campaign, and the results have been previously reported by Salo et al. (2019). The PM10 concentrations in the flue gas ranged from 0.2 to 10 mg m^{-3} whereas chemically analyzed mass concentrations of submicron primary particles varied between 0.005 and 3.3 mg m^{-3}. Organic particulate matter had clearly the highest contribution for primary (52–99%) submicron particles followed by sulfate (0.2–35%), chloride (0.4–8%), nitrate (0.02–5%) and ammonium (0.1–3%). Four primary emission experiments (Good 6 and Fair 1, Fair 3,

and Fair 8) had extremely low mass concentrations (5–12 μg m^{-3}, Fig. 2). The primary emission during poor combustion (Poor 5, Poor 10, and Poor 12) had clearly higher concentrations of POM (up to 3 mg m^{-3}, Fig. 2) which is consistent with the mass size distribution results (Fig. 1). A similar increase that was observed for POM due to poor burning conditions was not observed for the inorganic ions (sulfate, nitrate, ammonium, and chloride).

The mass concentrations of aged particles were considerably higher than those of primary ones indicating that large amounts of gaseous precursors existed in the flue gas that were subsequently oxidized in the PAM chamber and converted to particulate form. The aged PM was dominated by organic compounds with contributions of 72–99% followed by sulfate (8–22%). The contributions of other components in aged experiments were insignificant (Fig. 2).

3.3. Variability on particulate emissions

Due to the large variation in the mass concentrations and size distributions between and within the experiments, the differences between the experiments and possible instrumental reasons for these observations were further examined. Several reasons causing the high emissions levels during poor combustion (Poor 5, Poor 10, and Poor 12) when compared to other primary experiments (Fair 1, Fair 3, Good 6, and Fair 8) were identified. Firstly, during the poor combustion experiments that had high mass concentration the average raw gas CO$_2$ contribution in the flue gas, (indicating the used fuel amount, marked with black circles in Fig. 2) was higher (3–6 vol%) than during other primary runs (<2 vol %). However, this could not alone explain the big differences between the experiments (Fig. 2). Secondly, the additional adjustments in circulation of solid fuel rate or unstable fuel feeding rate that have an effect to the furnace temperature were likely influencing the emissions. The experiment Poor 10 with low burning temperature and low combustion efficiency had the highest POM emission. Large variation observed in the emission levels in general indicates that burning conditions had a large influence on the emissions of oil shale combustion. Thirdly, as shown in Chapter 3.1, the size distributions during low and high emission levels were different. The measurement size ranges influence on how the different instruments can measure the particles. The total mass concentration of submicron particles measured by the SMPS was different than obtained with the SP-AMS. The mass concentration

measured with the SMPS was on average twice as high as that measured with the SP-AMS, except in the experiment Fair 3, in which the mass concentration was much higher in the SPMS than in the SP-AMS (Table S1). In the experiment Fair 3, there was a significant contribution of mass in the size below 60 nm (Fig. 1), which was out of the SP-AMS optimal measurement size range. Also, the upper cut-off sizes of the instruments were different. For the SMPS and SP-AMS the cut off sizes were 414 nm (mobility diameter) and 700 nm (vacuum aerodynamic diameter), respectively. In conclusion, due to the small particle size, the mass concentrations observed in exhaust emissions were small especially in good and mainly in fair burning conditions and thus instruments measuring mass were not optimal for the emissions measurements in the oil shale combustion whereas poor burning conditions produced a large fraction of particles which were outside the measurement size range of the SMPS (Fig. 1).

3.4. Gaseous precursors and secondary emissions

The average concentrations of gaseous compounds (N_2O, NO_2, NO, NH_3, SO_2, aromatic and aliphatic VOCs) in the flue gas for different experiments are shown in Fig. 3. The concentrations of oxidized nitrogen compounds (N_2O and NO_2) and ammonia had less variation between the experiments than the concentrations of aromatic and aliphatic VOCs and SO_2 (Fig. 3). However, there was a good correlation between the furnace temperature and NO_x concentration (coefficient of determination r^2: 0.77). The higher the furnace temperature the more NO_x was produced whereas lower temperature produced more VOCs, especially aliphatic VOCs (Fig. S4). The latter one was not as clear as with NO_x, as there were a couple of experiments (Poor 10 and Poor 11) with low combustion temperature and low VOCs. The highest average VOC concentration was detected for the experiment Poor 9 in which the combustion temperature was low and not stable, whereas two lowest VOC concentrations were observed for the experiments with highest combustion temperatures and high combustion efficiency (Poor 5 and Poor 12, Table 1). Although VOC emissions were low with higher furnace temperatures in the experiments Poor 5 and Poor 12, those experiments had quite high POM concentrations (Fig. 2).

The concentration of measured aliphatic VOCs was significantly higher than the concentration of aromatic VOCs (Fig. 3 and Fig. S5). Detailed VOC analysis showed that propane followed by ethene and methane had the highest mass concentrations of the analyzed VOCs. For example, the contribution of propane to VOC was almost 80% in the experiments Fair 8 and Poor 9 (Fig. S6). The contribution of aromatic VOC, mainly xylene and benzene, varied between 9 and 40% of the analyzed VOCs (Figs. 3 and S6). Based on the chamber experiment study done by Ng et al. (2007), the observed SOA yield of these aromatic VOCs is typically in the range of 20–40%. If we use these yields in this study for

aged emission experiments, the measured concentrations of POM were close to the estimated ones, except in the experiment Poor 11, in which much higher concentration of secondary POM was formed compared to the estimated value (Fig. 4). The particle formation potential for aliphatic hydrocarbons with less than six carbon has been considered to be negligible except for isoprene (Seinfeld and Pandis, 2006).

3.5. Oxidation state of organic compounds

The Oxygen to Carbon ratio (O:C), which describes how oxidized POM is, varied from 0.06 to 0.35 for the primary experiments and from 0.51 to 0.89 for the aged experiments. The observed average Hydrogen to Carbon ratios (H:C) varied from 1.32 to 1.87 for primary emissions but were quite stable for secondary emissions (1.82–1.90; Table 2). The lowest O:C and POM to OC ratio (POM:OC) observed for aged particles (Poor 9) are resembling values typically measured downwind of the urban area (Aiken et al., 2008). POM:OC values close and above two, like observed for other aged experiments, are typical for non-urban aerosols (Aiken et al., 2008; Turpin and Lim, 2001). The estimated average density of POM (based on elemental ratios) for different experiments was 0.99–1.42 g cm^{-3}. Density followed the ratio of POM to OC (Table 2, Kuwata et al., 2012). For aged ambient oxygenated organic aerosol (OOA), the O:C may increase up to 1 (Aiken et al., 2008), but ranges typically between 0.5 and 0.8 depending on the volatility of the organic fraction (Canagaratna et al., 2015). The mass spectra of POM for aged Good 7 and Poor 9 with extreme O:C values and carbon oxidation state (OS_c, Kroll et al., 2011) are presented in Fig. S7. During the experiment Good 7, in which the burning conditions were good, the highest O:C, and the lowest concentration of POM were measured, whereas during the experiment Poor 9, the absolute amount of aromatic VOCs and also the concentrations of POM were the highest (Fig. S6), but the O:C was the lowest indicating that the oxidation process was still going on or too few oxidants were present.

For the primary experiments O:C varied from 0.06 to 0.35 and POM: OC from 1.23 to 1.59. The lowest values were measured when the concentrations of POM were high and the highest ones with low POM concentrations. The POM:OC values were lower than estimated for urban aerosols resembling more of primary emissions like e.g. hydrocarbon-like organic aerosol (HOA, Turpin and Lim, 2001; Canagaratna et al., 2015). The mass spectra of the experiment Poor 10 (Fig. S7) contained ions of $C_2H_3^+$, $C_2H_5^+$, $C_3H_5^+$, $C_3H_7^+$, $C_4H_7^+$ and $C_4H_9^+$, which have been typically observed for primary aerosols (e.g., Crippa et al., 2013), but resembled mostly of the oleic acid mass spectra (r^2:0.88) with two highest ions ($C_3H_5^+$ and $C_4H_7^+$) were both unsaturated organic ions. However, the mass spectra of the experiment Poor 10 had a higher fraction of aromatic ions. For comparison, the mass spectra of POM for the experiment Good 6, which was chosen to present good
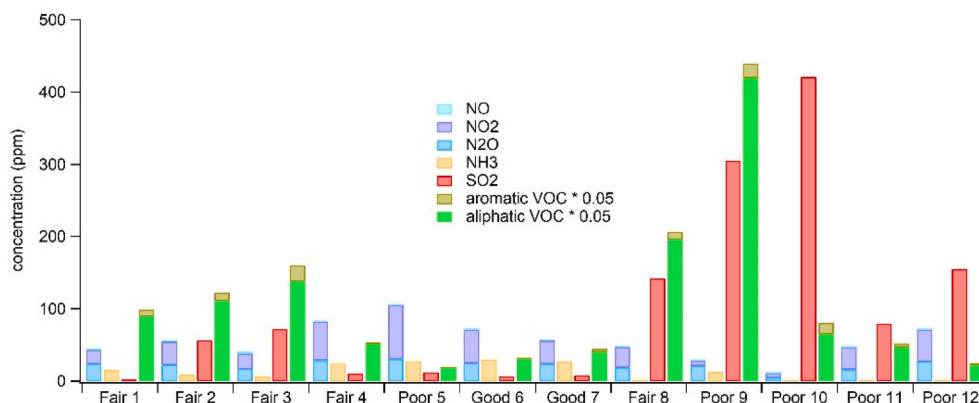

Fig. 3. Average concentrations of gaseous compounds (NO, NO_2, N_2O, NH_3, SO_2, VOCs) in different experiments during oil shale combustion. Aromatic VOCs include toluene, xylene, and benzene and aliphatic VOCs include CH_4, CH_2O, C_2H_4, C_2H_6, C_3H_8 and hexane.
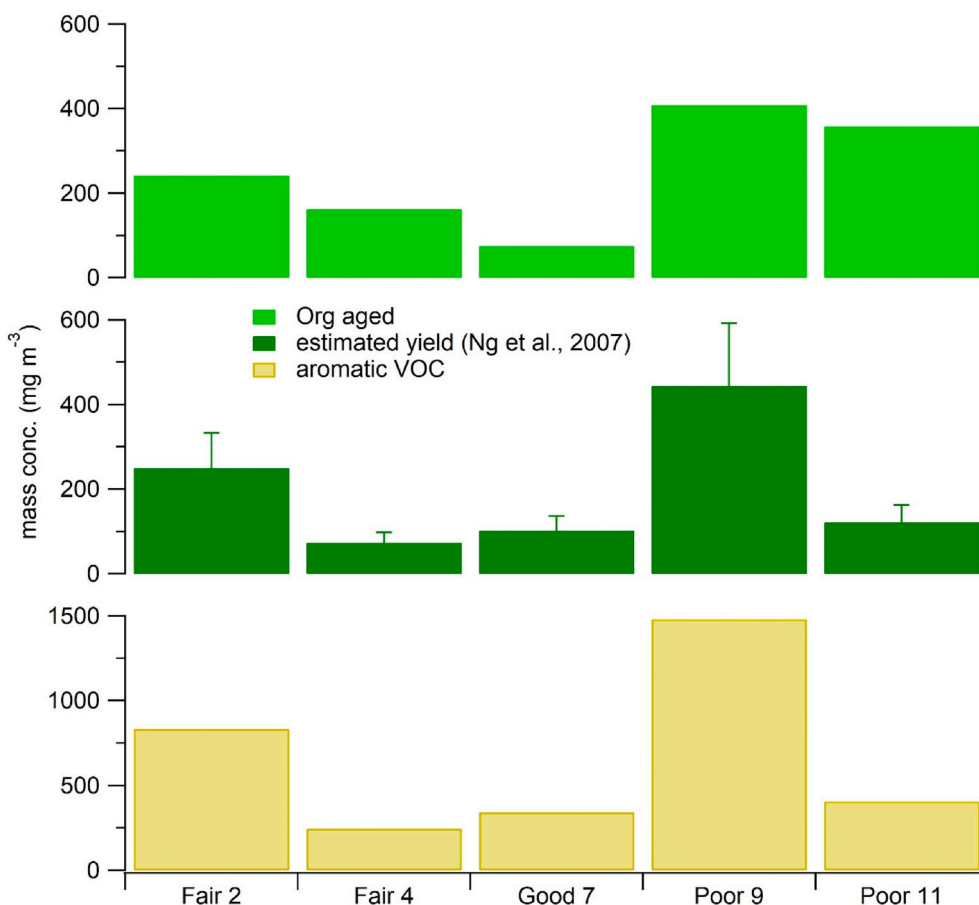
Fig. 4. Average concentrations of aromatic VOC (lower panel), estimated production (30%) of SOA from aromatic VOC (Ng et al., 2007, middle panel), and concentration of aged particulate organic matter measured after the PAM chamber (upper panel) during the oil-shale combustion. The error bars in the middle panel describe the variation of the estimated yields (20–40%).

Fig. 5. Sulfur dioxide, sulfuric acid, and particulate sulfate concentrations during different experiments. Fair 1, Fair 3, Poor 5, Good 6, Fair 8, Poor 10, and Poor 12 (on the left) present primary emissions and Fair 2, Fair 4, Good 7, Poor 9, and Poor 11 (on the right) present aged aerosol for sulfuric acid and sulfate. SO_2 presents primary emissions (measured before the PAM chamber).

burning conditions, are also presented in Fig. S7. Again, it is clearly seen that the burning conditions affect the amount of POM and to the state of oxidation. In summary, during poor combustion more incompletely burnt carbonaceous material is left and hence higher POM concentrations are seen in a case of primary emissions whereas during aged experiments new POM were formed from the precursor gases which increase the mass of the POM.

3.6. Evolution of sulfur components

Sulfur content in the burned oil shale was on average 1.6% (Table S2). Most of the released sulfur is expected to combine with free CaO and settle back to ash when oil shale is burnt, but some of it will oxidize first to SO_2 and further to SO_3, leading to formation of sulfuric acid, which can nucleate or condense to form particulate sulfate.

During the measurements, the SO_2 concentration varied between 2 and 440 ppm in different experiments. There was an indication that higher SO_2 concentrations were detected together with low furnace temperature, but this was not consistent (Fig. S4). The circulation rate of the solid fuel likely had an effect on the amount of released sulfur, but this could not be confirmed. In theory, if the circulation rate is too low, the binding of released sulfur with CaO does not take place. The SO_2 contribution to the measured sulfur components (SO_2, H_2SO_4 and sulfate) was mostly over 98% in primary emissions. Only a small contribution of sulfuric acid was formed during the primary emission measurements (Fig. 5), whereas on average 25% of SO_2 was oxidized to H_2SO_4 in the PAM chamber, but the observed variation was large. As the burning conditions and hence emissions varied a lot, more detailed sulfur chemistry was studied during the good burning conditions. The experiments Good 6 (primary) and Good 7 (aged) had stable and optimum furnace temperature in which the average SO_2 concentrations were 6.50 and 8.25 ppm, respectively. Note that SO_2 was measured only before the PAM chamber, so there was no measured evidence if any SO_2 was present after the flue gas had gone through the oxidation chamber in the experiment Good 7. As mentioned before, only a small amount of H_2SO_4 was formed during the oil shale combustion before or at the measurement point when primary particles were measured, whereas roughly 37 and 46% of SO_2 was oxidized to H_2SO_4 (measured by CI-APi-ToF) and particulate sulfate (measured by the SP-AMS), respectively, in the experiment Good 7 in which flue gases were directed through the oxidation chamber. It was unexpected that gaseous H_2SO_4 existed still after the PAM chamber. Also, a small amount of SO_2 was left after the PAM based on the subtraction of measured SO_4 (ppm) and H_2SO_4 (ppm) (after the PAM) from SO_2 (ppm) (before the PAM).

4. Conclusions

In this study, oil shale combustion measurements were conducted in the 60 kW Circulating Fluidized Bed (CFB) combustion test facility in Tallinn University of Technology, Estonia. Aerosol chemical composition, number and mass size distributions, organic and inorganic gases, and sulfuric acid molecules and clusters were studied using a large variety of state-of-the-art instruments (e.g., a Soot Particles Aerosol Mass Spectrometer, a nitrate ion based Chemical Ionization Atmospheric Pressure interface Time-of-Flight Mass Spectrometer) for primary and artificially aged emissions mimicking atmospheric secondary aerosol formation process.

Oil shale combustion was observed to produce a complex mixture of particulate and gaseous emissions. Burning conditions were observed to have a large influence on exhaust emissions. Good burning conditions produced lower particulate emissions and affected the size distributions of particles producing a large fraction of sub 10 nm sized particles. The poor burning conditions produced larger particles, the number size distribution peaking at 100 nm and thus significantly increased the particulate mass concentrations in exhaust emissions. Due to the small size of particles (10 nm) formed in the oil shale combustion during good

burning conditions, the mass-based instruments were not optimal for the emission measurements.

Large variation in gaseous emissions, especially SO_2 and VOCs were observed. The results confirmed that combustion conditions and temperature had a direct effect on emissions. In general, lower temperatures caused higher VOC emissions whereas higher temperature caused higher NO_x emissions.

The mass concentration of secondary emissions (aged particles), especially particulate organic matter (POM), was observed to be many orders of magnitude larger than primary emissions. Aged POM had higher density values, OC to POM ratio and oxidation state compared to primary POM. In addition, sulfate concentrations increased during oxidation although the increment was not as large as for POM. The oxidation process of sulfur was measured from gas phase (SO_2) to particulate sulfate via H_2SO_4-molecule and its clusters. On average 25% of SO_2 was oxidized to H_2SO_4 but the variation was large.

As the potential of oil shale emissions to produce secondary aerosol in the atmosphere is large, it is very important to take into account gaseous emissions when the emission mitigation systems or emission regulations for oil shale combustion are considered. However, with proper combustion conditions (temperature and circulation) the formation of gaseous pollutants can be significantly reduced. Also, particulate emissions can be reduced by optimizing the burning conditions.

CRediT authorship contribution statement

Minna Aurela: Formal analysis, Data curation, Acquisition of data, Analysis and interpretation of data, Writing – original draft, Writing – review & editing, Visualization. **Fanni Mylläri:** Formal analysis, Data curation, Acquisition of data, Analysis of data, Writing – review & editing. **Alar Konist:** Conceptualization, Conception and design of the study, Writing – review & editing, Methodology. **Sanna Saarikoski:** Formal analysis, Data curation, Analysis and interpretation of data, Writing – review & editing. **Miska Olin:** Formal analysis, Data curation, Analysis and interpretation of data, Writing – review & editing. **Pauli Simonen:** Funding acquisition, Formal analysis, Data curation, Acquisition of data, Analysis and interpretation of data, Writing – review & editing. **Matthew Bloss:** Funding acquisition, Data curation, Acquisition of data, Writing – review & editing. **Dmitri Nešumajev:** Funding acquisition, Data curation, Acquisition of data, Writing – review & editing. **Laura Salo:** Acquisition of data, Writing – review & editing. **Marek Maasikmets:** Funding acquisition, Data curation, Acquisition of data, Writing – review & editing. **Mikko Sipilä:** Formal analysis, Data curation, Writing – review & editing, Analysis and interpretation of data. **Miikka Dal Maso:** Formal analysis, Data curation, Analysis and interpretation of data, Writing – review & editing. **Jorma Keskinen:** Formal analysis, Data curation, Analysis and interpretation of data, Writing – review & editing. **Hilkka Timonen:** Conceptualization, Conception and design of the study, Writing – review & editing. **Topi Rönkkö:** Conceptualization, Conception and design of the study, Writing – review & editing, Supervision, All authors approve the version to be submitted.

Declaration of competing interest

The authors declare that they have no known competing financial interests or personal relationships that could have appeared to influence the work reported in this paper.

Acknowledgements

Appendix A. Supplementary data

Supplementary data to this article can be found online at https://doi.org/10.1016/j.aeaoa.2021.100139.

References

Aiken, A.C., DeCarlo, P.F., Kroll, J.H., Worsnop, D.R., Huffman, J.A., Docherty, K.S., Ulbrich, I.M., Mohr, C., Kimmel, J.R., Sueper, D., Sun, Y., Zhang, Q., Trimborn, A., Nirthway, M., Ziemann, P.J., Canagaratna, M.R., Onasch, T.B., Alfarra, M.R., Prevot, A.S.H., Dommen, J., Duplissy, J., Metzger, A., Baltensberger, U., Jimenez, J. F., 2008. O/C and OM/OC ratios of primary, secondary, and ambient organic aerosols with high-resolution time-of-flight Aerosol mass spectrometry. Environ. Sci. Technol. 42, 4478–4485. https://doi.org/10.1021/es703009q.

Andreae, M.O., Jones, C.D., Cox, P.M., 2005. Strong present-day aerosol cooling implies a hot future. Nature 435 (7046), 1187–1190. https://doi.org/10.1038/nature03671.

Canagaratna, M.R., Jayne, J.T., Jimenez, J.L., Allan, J.D., Alfarra, M.R., Zhang, Q., Onasch, T.B., Drewnick, F., Coe, H., Middlebrook, A., Delia, A., Williams, L.R., Trimborn, A.M., Northway, M.J., DeCarlo, P.F., Kolb, C.E., Davidovits, P., Worsnop, D.R., 2007. Chemical and microphysical characterization of ambient aerosols with the aerodyne aerosol mass spectrometer. Mass Spectrom. Rev. 26, 185–222. https://doi.org/10.1002/mas.20115.

Canagaratna, M.R., Jimenez, J.L., Kroll, J.H., Chen, Q., Kessler, S.H., Massoli, P., Hildebrandt Ruiz, L., Fortner, E., Williams, L.R., Wilson, K.R., Surratt, J.D., Donahue, N.M., Jayne, J.T., Worsnop, D.R., 2015. Elemental ratio measurements of organic compounds using aerosol mass spectrometry: characterization, improved calibration, and implications. Atmos. Chem. Phys. 15, 253–272. https://doi.org/10.5194/acp-15-253-2015, 2015.

Crippa, M., DeCarlo, P.F., Slowik, J.G., Mohr, C., Heringa, M.F., Chirico, R., Poulain, L., Freutel, F., Sciare, J., Cozic, J., Di Marco, C.F., Elsasser, M., Nicolas, J.B., Marchand, N., Abidi, E., Wiedensohler, A., Drewnick, F., Schneider, J., Borrmann, S., Nemitz, E., Zimmermann, R., Jaffrezo, J.-L., Prévôt, A.S.H., Baltensperger, U., 2013. Wintertime aerosol chemical composition and source apportionment of the organic fraction in the metropolitan area of Paris. Atmos. Chem. Phys. 13, 961–981. https://doi.org/10.5194/acp-13-961-2013.

COST Action CA16109 COLOSSAL Chemical On-Line cOmposition and Source Apportionment of fine aerosoL, Working Group 1. Guidelines for comparison of ACSM measurement with co-located external data. Deliverable 1.2. Released in December 2019. https://www.costcolossal.eu/.

Docherty, K.S., Jaoui, M., Corse, E., Jimenez, J.L., Offenberg, J.H., Lewandowski, M., Kleindienst, T.E., 2013. Collection efficiency of the aerosol mass spectrometer for chamber-generated secondary organic aerosols. Aerosol Sci. Technol. 47, 294–309. https://doi.org/10.1080/02786826.2012.752572.

EU, 2010. Directive 2010/75/EU of the European Parliament and of the Council of 24 November 2010 on Industrial Emissions. ELI: http://data.europa.eu/eli/dir/2010/75/2011-01-06.

Geller, M., Biswas, S., Sioutas, C., 2006. Determination of particle effective density in urban environments with a differential mobility analyzer and aerosol particle mass analyzer. Aerosol Sci. Technol. 40, 709–723. https://doi.org/10.1080/02786820600803925.

Happonen, M., Mylläri, F., Karjalainen, P., Frey, A., Saarikoski, S., Carbone, S., Hillamo, R., Pirjola, L., Häyrinen, A., Kytömäki, J., Niemi, J.V., Keskinen, J., Rönkkö, T., 2013. Size distribution, chemical composition, and hygroscopicity of fine particles emitted from an oil-fired heating plant. Environ. Sci. Technol. 47, 14468–14475. https://doi.org/10.1021/es4028056.

Jokinen, T., Sipilä, M., Junninen, H., Ehn, M., Lönn, G., Hakala, J., Petäjä, T., Mauldin III, R., Kulmala, M., Worsnop, D., 2012. Atmospheric sulphuric acid and neutral cluster measurements using CI-APi-TOF. Atmos. Chem. Phys. 12, 4117–4125. https://doi.org/10.5194/acp-12-4117-2012.

Junninen, H., Ehn, M., Petäjä, T., Luosujärvi, L., Kotiaho, T., Kostiainen, R., Rohner, U., Gonin, M., Fuhrer, K., Kulmala, M., Worsnop, D.R., 2010. A high-resolution mass spectrometer to measure atmospheric ion composition. Atmos. Meas. Tech. 3, 1039–1053. https://doi.org/10.5194/amt-3-1039-2010.

Kang, E., Root, M., Toohey, D., Brune, W., 2007. Introducing the concept of potential aerosol mass (PAM). Atmos. Chem. Phys. 7, 5727–5744. https://doi.org/10.5194/acp-7-5727-2007.

Karjalainen, P., Timonen, H., Saukko, E., Kuuluvainen, H., Saarikoski, S., Aakko-Saksa, P., Murtonen, T., Bloss, M., Dal Maso, M., Simonen, P., Ahlberg, E., Svenningsson, B., Brune, W.H., Hillamo, R., Keskinen, J., Rönkkö, T.(, 2016. Time-resolved characterization of primary particle emissions and secondary particle formation from a modern gasoline passenger car. Atmos. Chem. Phys. 16, 8559–8570. https://doi.org/10.5194/acp-16-8559-2016.

Konist, A., Pihu, T., Neshumayev, D., Külaots, I., 2013. Low grade fuel – oil shale and biomass co-combustion in CFB boiler. Oil Shale 30, 294–304. https://doi.org/10.3176/oil.2013.2S.09.

Konist, A., Järvik, O., Neshumayev, P.D., Pihu, T., 2019. Utilization of pyrolytic wastewater in oil shale fired CFBC boiler. J. Clean. Prod. 234, 487–493. https://doi.org/10.1016/j.jclepro.2019.06.213.

Kroll, J.H., Donahue, N.M., Jimenez, J.L., Kessler, S.H., Canagaratna, M.R., Wilson, K.R., Altieri, K.E., Mazzoleni, L.R., Wozniak, A.S., Bluhm, H., Mysak, E.R., Smith, J.D., Kolb, C.E., Worsnop, D.R., 2011. Carbon oxidation state as a metric for describing the chemistry of atmospheric organic aerosol. Nat. Chem. 3, 133–139. https://doi.org/10.1038/nchem.948.

Kürten, A., Rondo, L., Ehrhart, S., Curtius, J., 2012. Calibration of a chemical ionization mass spectrometer for the measurement of gaseous sulfuric acid. J. Phys. Chem. 116, 6375–6386. https://doi.org/10.1021/jp212123n.

Kuwata, M., Zorn, S.R., Martin, S.T., 2012. Using elemental ratios to predict the density of organic material composed of carbon, hydrogen, and oxygen. Environ. Sci. Technol. 46, 787–794. https://doi.org/10.1021/es202525q.

Lambe, A.T., Ahern, A.T., Williams, L.R., Slowik, J.G., Wong, J.P.S., Abbatt, J.P.D., Brune, W.H., Ng, N.L., Wright, J.P., Croasdale, D.R., Worsnop, D.R., Davidovits, P., Onasch, T.B., 2011. Characterization of aerosol photooxidation flow reactors: heterogeneous oxidation, secondary organic aerosol formation and cloud condensation nuclei activity measurements. Atmos. Meas. Tech. 4, 445–461. https://doi.org/10.5194/amt-4-445-201.

Lelieveld, J., Evans, J.S., Fnais, M., Giannadaki, D., Pozzer, A., 2015. The contribution of outdoor air pollution sources to premature mortality on a global scale. Nature 525, 367–371. https://doi.org/10.1038/nature15371.

Lipsky, E., Robinson, A., 2006. Effects of dilution on fine particle mass and partitioning of semivolatile organics in diesel exhaust and wood smoke. Environ. Sci. Technol. 40, 155–162. https://doi.org/10.1021/es050319p.

Maaten, B., Järvik, O., Pihl, O., Konist, A., Siirde, A., 2020. Oil shale pyrolysis products and the fate of sulfur. Oil Shale 37, 51–69. https://doi.org/10.3176/oil.2020.1.03.

Martins, M., Salvador, S., Thovert, J.-F., Debenest, G., 2010. Co-current combustion of oil shale – Part 1: characterization of the solid and gaseous products. Fuel 89 (1), 144–151. https://doi.org/10.1016/j.fuel.2009.06.036.

Middlebrook, A.M., Bahreini, R., Jimenez, J.L., Canagaratna, M.R., 2012. Evaluation of composition-dependent collection efficiencies for the aerodyne aerosol mass spectrometer using field data. Aerosol Sci. Technol. 46, 258–271. https://doi.org/10.1080/02786826.2011.620041.

Mylläri, F., Asmi, E., Anttila, T., Saukko, E., Vakkari, V., Pirjola, L., Hillamo, R., Laurila, T., Häyrinen, A., Rautiainen, J., Lihavainen, H., O'Connor, E., Niemelä, V., Keskinen, J., Dal Maso, M., Rönkkö, T., 2016. New particle formation in the fresh flue-gas plume from a coal-fired power plant: effect of flue-gas cleaning. Atmos. Chem. Phys. 16, 7485–7496. https://doi.org/10.5194/acp-16-7485-2016.

Mylläri, F., Karjalainen, P., Taipale, R., Aalto, P., Häyrinen, A., Rautiainen, J., Pirjola, L., Hillamo, R., Keskinen, J., Rönkkö, T., 2017. Physical and chemical characteristics of flue-gas particles in a large pulverized fuel-fired power plant boiler during co-combustion of coal and wood pellets. Combust. Flame 176, 554–566. https://doi.org/10.1016/j.combustflame.2016.10.027.

Ng, N.L., Kroll, J.H., Chan, A.W.H., Chhabra, P.S., Flagan, R.C., Seinfeld, J.H., 2007. Secondary organic aerosol formation from m-xylene, toluene, and benzene. *Atmos. Chem. Phys.* 7, 3909–3922. https://doi.org/10.5194/acp-7-3909-2007.

Onasch, T.B., Trimborn, A., Fortner, E.C., Jayne, J.T., Kok, G.L., Williams, L.R., Davidovits, P., Worsnop, D.R., 2012. Soot particle aerosol mass spectrometer: development, validation, and initial application. Aerosol Sci. Technol. 46, 804–817. https://doi.org/10.1080/02786826.2012.663948.

Parve, T., Loosaar, J., Mahhov, M., Konist, A., 2011. Emission of fine particulates from oil shale fired large boilers. Oil Shale 28, 152–161. https://doi.org/10.3176/oil.2011.1S.07.

Peng, Z., Jimenez, J.L., 2020. Radical chemistry in oxidation flow reactors for atmospheric chemistry research. Chem. Soc. Rev. 49, 2570–2616. https://doi.org/10.1039/C9CS00766K.

Pihu, T., Neshumayev, D., Loo, L., Molodtsov, A., Valtsev, A., 2017. Full-scale tests on the co-firing of peat and oil shale in an oil shale fired circulating fluidized bed boiler. Oil Shale 34, 250–262. https://doi.org/10.3176/oil.2017.3.04.

Poulain, L., Birmili, W., Canonaco, F., Crippa, M., Wu, Z.J., Nordmann, S., Spindler, G., Prévôt, A.S.H., Wiedensohler, A., Herrmann, H., 2014. Chemical mass balance of 300 degrees C non-volatile particles at the tropospheric research site Melpitz, Germany. Atmos. Chem. Phys. 14, 10145–10162. https://doi.org/10.5194/acp-14-10145-2014.

Salo, L., Mylläri, F., Maasikmets, M., Niemelä, V., Konist, A., Vainumäe, K., Kupri, H.-L., Titova, R., Simonen, P., Aurela, M., Bloss, M., Keskinen, J., Timonen, H., Rönkkö, T., 2019. Emission measurements with gravimetric impactors and electrical devices: an aerosol instrument comparison. Aerosol Sci. Technol. 53, 526–539. https://doi.org/10.1080/02786826.2019.1578858.

Seinfeld, J.H., Pandis, S.N., 2006. Atmospheric Chemistry and Physics: from Air Pollution to Climate Change, second ed. John Wiley& Sons, Inc., Hoboken, New Jersey, USA.

Strizhakova, Y.A., Usova, T.V., 2008. Current trends in the pyrolysis of oil shale: a review. Solid Fuel Chem. 42, 197–201. https://doi.org/10.3103/S0361521908040022.

Timonen, H., Karjalainen, P., Saukko, E., Saarikoski, S., Aakko-Saksa, P., Simonen, P., Murtonen, T., Dal Maso, M., Kuuluvainen, H., Bloss, M., Ahlberg, E., Svenningsson, B., Pagels, J., Brune, W.H., Keskinen, J., Worsnop, D.R., Hillamo, R., Rönkkö, T., 2017. Influence of fuel ethanol content on primary emissions and secondary aerosol formation potential for a modern flex-fuel gasoline vehicle. Atmos. Chem. Phys. 17, 5311–5329. https://doi.org/10.5194/acp-17-5311-2017, 2017.

Turpin, B., Lim, H.-L., 2001. Species contributions to PM2.5 mass concentrations: revisiting common assumptions for estimating organic mass. Aerosol Sci. Technol. 35, 602–610. https://doi.org/10.1080/02786820119445.

Willis, M.D., Lee, A.K.Y., Onasch, T.B., Fortner, E.C., Williams, L.R., Lambe, A.T., Worsnop, D.R., Abbatt, J.P.D., 2014. Collection efficiency of the soot-particle aerosol mass spectrometer (SP-AMS) for internally mixed particulate black carbon. Atmos. Meas. Tech. 7, 4507–4516. https://doi.org/10.5194/amt-7-4507-2014.